

UC Riverside

UC Riverside Previously Published Works

Title

Resolving the Model-Observation Discrepancy in the Mesospheric and Stratospheric HOx Chemistry

Permalink

<https://escholarship.org/uc/item/1q15c9ch>

Journal

Earth and Space Science, 4(9)

ISSN

2333-5084

Authors

Li, King-Fai
Zhang, Qiong
Wang, Shuhui
[et al.](#)

Publication Date

2017-09-01

DOI

10.1002/2017ea000283

Copyright Information

This work is made available under the terms of a Creative Commons Attribution-NonCommercial-NoDerivatives License, available at <https://creativecommons.org/licenses/by-nc-nd/4.0/>

Peer reviewed



RESEARCH ARTICLE

10.1002/2017EA000283

Key Points:

- The kinetic rate coefficients and photo absorption coefficients are adjusted to better simulate the observed middle atmospheric OH and HO₂
- The model-observation discrepancy is reduced by adjusting the rate of H + O₂ + M → HO₂ + M and the O₂ absorption cross section at Lyman α
- A hitherto unsuspected radiative association reaction, H + O₂ → HO₂ + hv, may play a significant role in the mesospheric HO_x chemistry

Supporting Information:

- Supporting Information S1

Correspondence to:

K.-F. Li,
king-fai.li@ucr.edu

Citation:

Li, K.-F., Zhang, Q., Wang, S., Sander, S. P., & Yung, Y. L. (2017). Resolving the model-observation discrepancy in the mesospheric and stratospheric HO_x chemistry. *Earth and Space Science*, 4. <https://doi.org/10.1002/2017EA000283>

Received 12 APR 2017

Accepted 28 AUG 2017

Accepted article online 4 SEP 2017

Resolving the Model-Observation Discrepancy in the Mesospheric and Stratospheric HO_x Chemistry

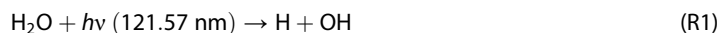
King-Fai Li^{1,2} , Qiong Zhang³ , Shuhui Wang⁴, Stanley P. Sander⁵ , and Yuk L. Yung³

¹Department of Applied Mathematics, University of Washington, Seattle, WA, USA, ²Department of Environmental Sciences, University of California, Riverside, CA, USA, ³Division of Geological and Planetary Sciences, California Institute of Technology, Pasadena, CA, USA, ⁴Joint Institute for Regional Earth System Science and Engineering, University of California, Los Angeles, CA, USA, ⁵Jet Propulsion Laboratory, California Institute of Technology, Pasadena, CA, USA

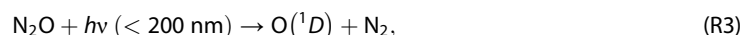
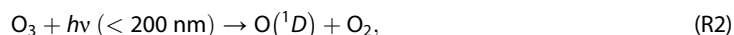
Abstract We examine the middle atmospheric odd-hydrogen (HO_x) chemistry by comparing the Aura Microwave Limb Sounder (MLS) OH and HO₂ measurements with a photochemical model simulation. The model underestimates mesospheric OH and HO₂ concentrations if the standard chemical kinetic rates are used, whether the model H₂O and O₃ are constrained with observations or not. To resolve the discrepancies, we adjust the kinetic rate coefficients of three key reactions (O + OH → O₂ + H, OH + HO₂ → H₂O + O₂, and H + O₂ + M → HO₂ + M) and the O₂ photo absorption cross section at Lyman α (121.57 nm) using the Bayesian optimal estimation. A much better model-observation agreement can be achieved if the kinetic rate coefficients for H + O₂ + M → HO₂ + M is increased by 134–310%, and the O₂ photo absorption cross section at Lyman α is reduced by 33–54%, while the kinetic rate coefficients for O + OH → O₂ + H and OH + HO₂ → H₂O + O₂ remain consistent with the current laboratory values. The kinetic rate coefficient for H + O₂ + M → HO₂ + M requires a very large adjustment beyond the uncertainty limits recommended in the NASA Data Evaluation, suggesting the need for future laboratory measurements. An alternative explanation is that the radiative association reaction, H + O₂ → HO₂ + hv, plays a significant role, which has never been measured. Our results demonstrate that high-quality satellite observations can be used to constrain photochemical parameters and help improve our understanding of atmospheric chemistry.

1. Introduction

Odd hydrogen (HO_x) species, including hydroxyl radical (OH) and hydroperoxyl (HO₂), are important catalysts of odd oxygen in the middle atmosphere (Brosseur & Solomon, 2005). The main source of middle atmospheric HO_x is direct photolysis of H₂O by the solar Lyman α line in the mesospheric region (>60 km):



or the photolysis of O₃ and N₂O by solar UV below 200 nm and 330 nm, respectively, in the stratospheric region (<60 km) that produces O(¹D):



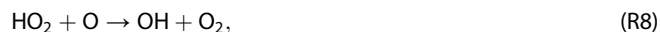
followed by



©2017. The Authors.

This is an open access article under the terms of the Creative Commons Attribution-NonCommercial-NoDerivs License, which permits use and distribution in any medium, provided the original work is properly cited, the use is non-commercial and no modifications or adaptations are made.

OH is then converted to HO₂, and vice versa, via reactions with O, O₃, and NO:



Throughout the whole middle atmosphere, the ultimate sink of HO_x is through



(Brasseur & Solomon, 2005; Canty & Minschwaner, 2002). Reactions (R1)–(R3) show that the net source of HO_x is sensitive to variations of incoming solar UV solar spectral irradiance (SSI). Satellite observations suggest that the HO_x species better correlate with SSI than O₃ or temperature (Rozanov et al., 2006) and are good indicators of solar cycle with almost zero time lag (Shapiro et al., 2012; Wang et al., 2015).

The HO_x profiles have been observed using balloon-based measurements (Englert et al., 2000; Heaps & McGee, 1985; Jucks et al., 1998; Kendall & Clark, 1980; Park & Carli, 1991; Pickett & Peterson, 1993; Traub et al., 1990), ground-based measurements (Burnett & Burnett, 1981; Cageao et al., 2001; Iwagami et al., 1995), and rocket-borne (Anderson, 1971) and space-borne measurements (Conway et al., 1999; Pickett, 2006). Despite the above simple HO_x photochemistry in the stratosphere and mesosphere, a number of studies reveal discrepancies between observed and simulated HO_x concentrations. Conway et al. (2000) first claimed that the simulated stratospheric OH is lower than that observed by the Middle Atmosphere High Resolution Spectrograph Investigation (MAHRSI) (Summers et al., 1997), while the simulated mesospheric OH is higher. They thus coined the term “HO_x dilemma” to describe this discrepancy having opposite signs in the stratosphere and mesosphere. Later, this apparent dilemma has been attributed to large uncertainties of MAHRSI data at low altitudes (Englert et al., 2008). However, other model-observation discrepancies persist. For example, Millán et al. (2015) showed that the standard photochemistry significantly underestimates the mesospheric HO₂ at 70 km observed by Microwave Limb Sounder (MLS) (Livesey et al., 2015; Pickett et al., 2006; Pickett et al., 2008) and the HO₂ discrepancy disappeared only when the observed OH was used to constrain the model. One possible cause of the aforementioned model-observation discrepancy in the HO_x concentrations may be model biases due to laboratory uncertainties of chemical kinetics rates (Sander et al., 2011). A number of groups (e.g., Canty et al., 2006; Conway et al., 2000; Jucks et al., 1998; Siskind et al., 2013; Summers et al., 1997) tried to adjust the kinetic rates of some important photochemical reactions to better fit the simulated HO_x with the observations. However, the choices of the photochemical reactions to be adjusted are not unique. Table 1 lists the reactions adjusted by some of the previous groups. For example, Canty et al. (2006) adjusted the reaction rates for OH + HO₂ → H₂O + O₂ (R10) and



while Siskind et al. (2013) adjusted the reaction rate for



The adjustments of the reaction rates also vary significantly among different studies. To have a more objective choice of reactions to be adjusted, we shall adopt a Bayesian optimal estimation approach

Table 1
 Perturbations (in %) of Kinetic Rate Coefficients in Previous Studies and the Current Study

	Summers97 ^a		Jucks98 ^b		Conway00 ^c	Canty06 ^d	Siskind13 ^e	This work ^f			
	B	C	D	D1 ^k	B ^l			I ⁿ	II ⁿ	III ⁿ	IV ^o
H ₂ O + O(¹ D) ^g				+25							
OH + O ^h				+25	(-50)	+20 ^m		(-53)	(-31)	(-15)	+12
HO ₂ + O	(-50)	(-20)	(-25)								
OH + HO ₂		+30	(-25)			+20		+30	(-13)	(-15)	(-10)
H + O ₂ + M ⁱ							+52 ^p		+131	+134	+310
O ₂ + hν ^j										(-54)	(-33)
Ly α							+8				

Note. The previous studies included here are Summers et al. (1997) (Summers97), Jucks et al. (1998) (Jucks98), Conway et al. (2000) (Conway00), Canty et al. (2006) (Canty06), and Siskind et al. (2013) (Siskind13). Summers et al. (1997) defined their Models B and C in the sixth paragraph of their text. Jucks et al. (1998) defined their Model D in the figure caption of their Figure 2; Model D1 is a code name we assign to the alternative model described in the eighth paragraph of Jucks et al.'s (1998) "Discussion" section. Conway et al. (2000) defined their Model B in the figure caption of their Plate 2. For this work, Experiments I-IV are defined in section 3.3. For better visualization, negative values are quoted in parentheses.

^aBased on JPL1994 Evaluation (DeMore et al., 1994). ^bBased on JPL1994 Evaluation. Model H₂O, O₃, and temperature were constrained. ^cBased on JPL1997 Evaluation (DeMore et al., 1997). Model H₂O, O₃ (below 47 km), N₂O, NO_y, CH₄, Cl_y, and temperature were constrained. ^dBased on JPL2002 Evaluation. Model H₂O, O₃, N₂O, CO, and temperature were constrained. ^eBased on JPL2011 Evaluation. Model H₂O and temperature were constrained. ^fBased on JPL2011 Evaluation. ^g*k*_{H₂O+O(1D)} in JPL2006 (Sander et al., 2006) and JPL2011 (Sander et al., 2011) Evaluations are 5% larger than JPL2002 Evaluation (Sander et al., 2002) at 170 K. ^h*k*_{OH+O} in JPL2011 is 16% larger than JPL2006 and JPL2002 at 170 K. ⁱ*k*_{H+O₂+M} in JPL2006 and JPL2011 are 36% less than JPL2002 at 170 K. ^jO₂ photo absorption cross section at Lyman α, resolved by a spectral resolution 0.1 nm at 121.57 nm in the 1-D photochemical model. ^kThis experiment was not labeled in Jucks et al. (1998) but was discussed in the eighth paragraph of their Discussions section. ^lConway et al. (2000) presented two other models: Models C and D, which were equivalent to Summers et al.'s (1997) Model C and Jucks et al.'s (1998) Model D, respectively. ^mEquivalent to 4% increase of JPL2011. ⁿNo observational constraints have been applied. ^oModel H₂O and O₃ between 30 and 72 km have been constrained by MLS observations. ^pEquivalent to JPL2002 and Wong and Davis (1974).

that accounts for both observational and model uncertainties to adjust the photochemical model parameters. Our approach is to set up an inverse problem, where parameters of the forward model (i.e., the photochemical model) would be estimated given the MLS observations. Below, we refer to the term "inversion" in a broad sense for the search of the model parameter values that would minimize a cost function defined in terms of observations and forward model outputs. When the observation is a set of satellite spectral measurements and the model parameter is the vertical profile of an atmospheric tracer (e.g., stratospheric ozone), for instance, then the search for the vertical profile is also known as "satellite retrieval" (Rodgers, 2000). In applied mathematics, an "inversion" described above is also known as an "optimization" of model parameters.

A number of studies (e.g., Canty et al., 2006; Siskind et al., 2013; Summers et al., 1997) attempted to relate the model-observation discrepancy in HO_x to the O₃ deficit problem, which is beyond the scope of this work. Our focus here is to apply an inversion method to atmospheric chemical modeling, emphasizing how to choose an appropriate set of reactions to be optimized and how to interpret the inversion results.

The rest of the paper is organized as follows. Section 2 presents the data and the photochemical model to be used in the inverse problem. Section 3 describes the inversion algorithm and presents the results. We will identify the need for reconsiderations of the laboratory data and recommended rate coefficients for H + O₂ + M → HO₂ + M (R12). Discussions and conclusions follow in section 4.

2. Data and Model

2.1. MLS Data

The MLS instrument aboard the Aura spacecraft was launched in 2004 (Waters et al., 2006) into a Sun-synchronous orbit, crossing the equator at around 1:45 A.M./P.M. We shall use the MLS version 4.2 daytime OH data (zonally and tropically averaged over 25°S and 25°N) during June 2005. This period was the first summer, having the strongest solar activity after launch; this choice of the period ensures that the measured HO_x concentrations have the highest signal-to-noise ratio. For the purpose of inversion, we interpolate the MLS profiles to the model levels that are uniformly separated by 2 km from ground to 120 km (see section 2.2). For quality control, the observed OH profile between 26 and 82 km (29 levels) and the observed HO₂ profiles between 38 and 82 km (23 levels) are used in the inversion.

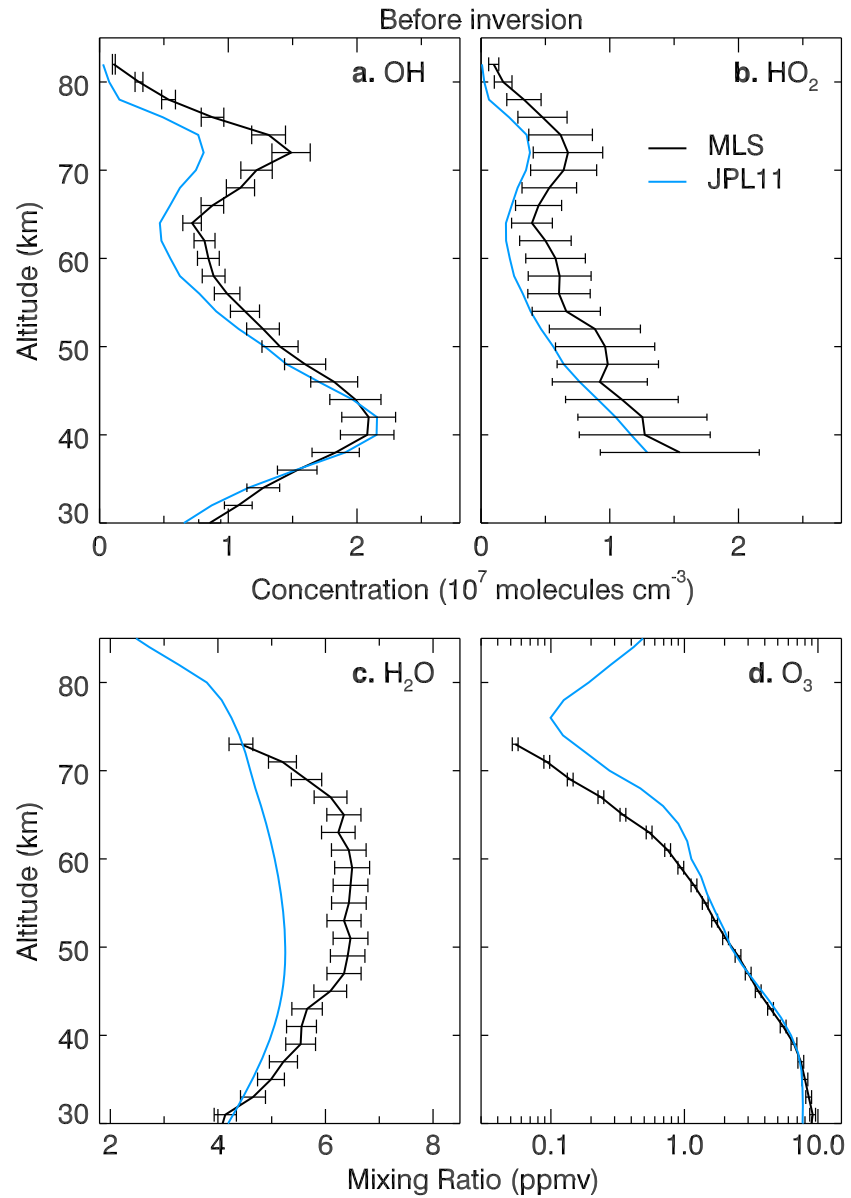


Figure 1. Comparison between MLS 1:45 P.M. measurements (black) and 1-D model simulations (blue): (a) OH, (b) HO₂, (c) H₂O, and (d) O₃. MLS daytime measurements are averaged between 25°S and 25°N from 1 to 30 June 2005. The blue curves show the model results using the kinetic rate coefficients from the 2011 JPL Data Evaluation. For visualization, H₂O and O₃ mixing ratios are shown. For OH, H₂O, and O₃, we assume a systematic error of 5%. For HO₂, we assume a systematic error of 20%.

where various observed concentrations of H₂O and O₃, as well as minor species such as N₂O, NO_y, CH₄, and Cl_y, have been used to constrain the model calculations; see the footnotes in Table 1. A problem with our unconstrained calculation is that the simulated H₂O and O₃ profiles may be different from the observed ones, as shown in Figures 1c and 1d: the simulated H₂O mixing ratio is at least 20% less than the MLS H₂O over altitudes between 44 and 72 km, and the simulated O₃ mixing ratio is about 50% less than the MLS O₃ between 60 km and 72 km. To illustrate the effect of the observational constraints on the retrieved kinetic rates, we perform another experiment (Experiment IV), where the model H₂O and O₃ profiles between 30 km and 72 km are fixed with the MLS observation. Experiment IV is similar to the model simulation conducted by Millán et al. (2015).

The model is run until the OH and HO₂ profiles at 1:45 P.M. over the equator (0°N) become steady. Analogous to \mathbf{y} , we define a model vector \mathbf{y}_m that concatenates the simulated OH and HO₂ profiles:

$$\mathbf{y}_m = \begin{bmatrix} \text{OH}(26 \text{ km}) \\ \vdots \\ \text{OH}(82 \text{ km}) \\ \text{HO}_2(38 \text{ km}) \\ \vdots \\ \text{HO}_2(82 \text{ km}) \end{bmatrix}_{\text{model}} \quad (4)$$

2.3. Discrepancies Between Observed and Model OH and HO₂ Profiles

Figures 1a and 1b show the monthly mean zonal-mean MLS OH and HO₂ profiles averaged between 25°S and 25°N in June 2005 (black lines). The use of a monthly mean minimizes the effects of the 27 day solar cycle. The simulated OH and HO₂ profiles (blue lines) are compared with the MLS observations. Three differences are noted. (1) The simulated mesospheric OH and HO₂ at 72 km are significantly underestimated, both only half of the observed, consistent with Millán et al.'s (2015) conclusion; (2) the simulated stratospheric OH at 40 km is slightly more than observed but they agree within the measurement uncertainty, consistent with Canty et al.'s (2006) conclusion; and (3) the simulated stratospheric HO₂ at 40 km is less than observed but they agree within the measurement uncertainty. Figures 1c and 1d show the simulated H₂O and O₃ profiles, as discussed in section 2.2. We assume a systematic error of 5% for both MLS H₂O and O₃ measurements.

Below we will test whether the model-observation differences can be improved by adjusting some of the reaction rates in the inversion.

3. Inversion of Kinetic Rates

Benefited from the simplicity of the HO_x photochemistry, we limit our parametric study to reaction rate constants and assume that the uncertainties of atmospheric transport and ambient temperature are not dominant. As in previous works (e.g., Canty et al., 2006; Pickett et al., 2008; Siskind et al., 2013), we will adjust the reaction rates A of some "important" chemical reactions for HO_x to minimize the discrepancy between the simulated and observed OH and HO₂ profiles. The same adjustment of A is applied to all model levels. E_d/R and T remain unchanged during the inversion.

3.1. Jacobians and Selection of Reactions

When the kinetic rate of a reaction is adjusted, the vertical profiles of OH and HO₂ will change. The partial derivative of the vertical profiles with respect to the kinetic rate defines the sensitivity of OH or HO₂ to the associated reaction. The collection of the partial derivatives form a 52×176 Jacobian matrix:

$$\mathbf{K} = \begin{bmatrix} \frac{\partial \mathbf{y}_m}{\partial A_1} & \dots & \frac{\partial \mathbf{y}_m}{\partial A_{176}} \end{bmatrix} = \begin{bmatrix} \frac{\partial[\text{OH}]_{26 \text{ km}}}{\partial A_1} & \dots & \frac{\partial[\text{OH}]_{26 \text{ km}}}{\partial A_{176}} \\ \vdots & & \vdots \\ \frac{\partial[\text{OH}]_{82 \text{ km}}}{\partial A_1} & \dots & \frac{\partial[\text{OH}]_{82 \text{ km}}}{\partial A_{176}} \\ \frac{\partial[\text{HO}_2]_{38 \text{ km}}}{\partial A_1} & \dots & \frac{\partial[\text{HO}_2]_{38 \text{ km}}}{\partial A_{176}} \\ \vdots & & \vdots \\ \frac{\partial[\text{HO}_2]_{82 \text{ km}}}{\partial A_1} & \dots & \frac{\partial[\text{HO}_2]_{82 \text{ km}}}{\partial A_{176}} \end{bmatrix}, \quad (5)$$

where A_i is the rate coefficient of the i th reaction. As an example, $\frac{\partial[\text{OH}]_{26 \text{ km}}}{\partial A_{\text{OH}+\text{HO}_2}}$ is defined as the percent change in the OH concentrations at 26 km due to a 100% increase in the kinetic rate for the sink process $\text{OH} + \text{HO}_2 \rightarrow \text{H}_2\text{O} + \text{O}_2$.

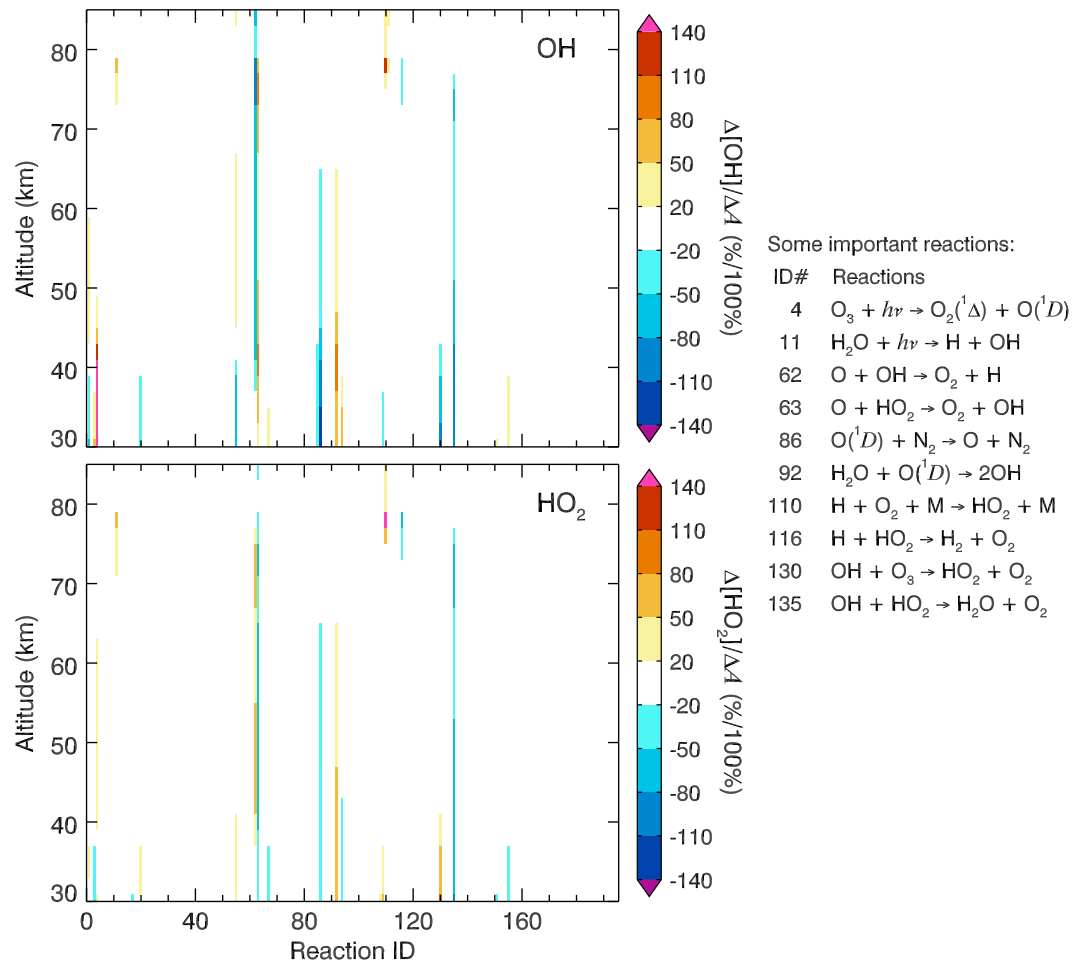


Figure 2. The Jacobian of (top) OH and (bottom) HO₂ with respect to reaction rate constants. The Jacobian at a particular altitude is defined as the percent change in OH or HO₂ concentration per 100% change in the reaction rate coefficient. Reaction ID are listed in the supporting information.

The selection of reactions to be adjusted is based on **K**, shown as partial derivatives of OH and HO₂ in Figure 2. The following HO_x reactions are found to have significant partial derivatives at 40 km and 72 km where the stratospheric and mesospheric peaks of HO_x are located: O + HO₂ → O₂ + OH, OH + HO₂ → H₂O + O₂, O + OH → O₂ + H, H + O₂ + M → HO₂ + M, and H + HO₂ → H₂ + O₂. These reactions may be candidates for the inversion. However, only some of them can be used. This is not only because of the limited number of degrees of freedom to be derived in section 3.2 but also because of “inherent degeneracy” under the context of inversion: the partial derivatives of some reactions may have similar vertical structures, e.g., having peaks at similar altitudes. A simple example of inherent degeneracy is the two reactions among odd-oxygen species and oxygen gas that have almost symmetrically opposite effects on both OH and HO₂: O + O₂ + M → O₃ + M, O + O₃ → 2O₂. The adjustments of values of A for these two reactions would not be unique, albeit the same changes in OH and HO₂ may be obtained. Therefore, in the selection process, we need to avoid selecting reactions that have structurally similar Jacobians. As the reactions O + OH → O₂ + H and O + HO₂ → O₂ + OH have similar Jacobians (Figures 3a and 3b), only one of them should be used in the inversion. For the same reason, since the reaction H + HO₂ → H₂ + O₂ has a Jacobian (Figure 3c) that is similar to that of H + O₂ + M → HO₂ + M (not shown), we will not include the former reaction in the inversion.

3.2. Bayesian Optimal Estimation

We adopt the Bayesian optimal estimation to retrieve the reaction rate coefficients (Rodgers, 2000). The recommended reaction rate coefficients in the 2011 JPL Data Evaluation will be used as the a priori values

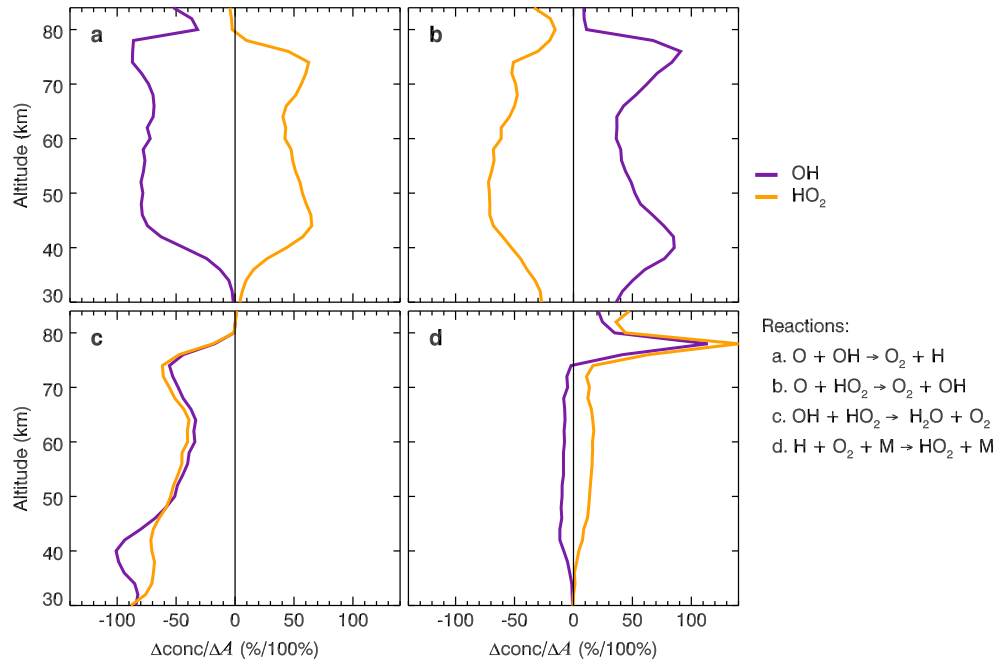


Figure 3. The Jacobians of OH (purple) and HO₂ (orange) with respect to the labeled kinetic rate coefficients.

for A . The a priori uncertainties of A are given by $[f(T) - 1] \times 100\%$, where $f(T)$ is an uncertainty scaling function defined in sections 1.2 and 2.6 of Sander et al. (2011), and $f(T)$ generally lies within 10–30% (but it can be as large as 200% for some reactions). We define a diagonal a priori error covariance matrix as

$$\mathbf{S}_a = \begin{bmatrix} (f_1 - 1)^2 & & 0 \\ & \ddots & \\ 0 & & (f_{176} - 1)^2 \end{bmatrix}. \quad (6)$$

One cannot choose an arbitrary number of reactions for inversion because the MLS observations may not have sufficient degrees of freedom to constrain a large number of model parameters. The degree of freedom of the MLS measurements is defined as (Rodgers, 2000)

$$d_s = \text{Tr}(\mathbf{K}\mathbf{S}_a\mathbf{K}^T [\mathbf{K}\mathbf{S}_a\mathbf{K}^T + \mathbf{S}_e]^{-1}), \quad (7)$$

where $\text{Tr}(\mathbf{M})$ is the trace, i.e., the sum of the diagonal elements, of a square matrix \mathbf{M} . d_s measures how many model parameter can be adjusted independently when fitting the MLS OH and HO₂ profiles. As a rough estimate, we assume $(f - 1) \approx 20\%$ for all reactions and obtain $d_s = 6.84$. Therefore, no more than seven reactions can be adjusted in the optimal estimation.

After the selection of reactions, the reaction rates of the selected reactions are to be adjusted such that the following Bayesian cost function is minimized

$$\chi^2 = [\mathbf{y} - \mathbf{y}_m(\mathbf{x})]^T \mathbf{S}_e^{-1} [\mathbf{y} - \mathbf{y}_m(\mathbf{x})] + (\mathbf{x} - \mathbf{x}_a)^T \tilde{\mathbf{S}}_a^{-1} (\mathbf{x} - \mathbf{x}_a), \quad (8)$$

where \mathbf{x} is a state vector containing the reaction rate coefficients to be adjusted, \mathbf{x}_a contains the a priori reaction rate coefficients corresponding to those in \mathbf{x} , $\tilde{\mathbf{S}}_a$ is the reduced a priori covariance

Table 2
The A Priori Uncertainties (1σ) of the Reaction Coefficients to be Adjusted

Reaction	Prior uncertainty
$O + OH \rightarrow O_2 + H$	15%
$OH + HO_2 \rightarrow H_2O + O_2$	15%
$H + O_2 + M \rightarrow HO_2 + M$	30%
O_2 photo absorption at Lyman α	30%

Note. The uncertainties of $O + OH \rightarrow O_2 + H$, $OH + HO_2 \rightarrow H_2O + O_2$, and $H + O_2 + M \rightarrow HO_2 + M$ are based on the JPL 2011 Evaluation (Sander et al., 2011). The uncertainty for the O_2 photo absorption cross section at Lyman α is heuristically derived; see text.

matrix with the selected reactions only, and $\mathbf{y}_m(\mathbf{x})$ is \mathbf{y}_m given \mathbf{x} . For example, if $O + OH \rightarrow O_2 + H$ and $O + HO_2 \rightarrow O_2 + OH$ are to be adjusted, then $\mathbf{x} = [A_{O+OH}, A_{OH+HO_2}]$, and $\tilde{\mathbf{S}}_a = \begin{bmatrix} (f_{O+OH} - 1)^2 & 0 \\ 0 & (f_{OH+HO_2} - 1)^2 \end{bmatrix}$. A reduced Jacobian $\tilde{\mathbf{K}}$ can be similarly defined: $\tilde{\mathbf{K}} = \begin{bmatrix} \frac{\partial \mathbf{y}_m(\mathbf{x})}{\partial A_{O+OH}} & \frac{\partial \mathbf{y}_m(\mathbf{x})}{\partial A_{OH+HO_2}} \end{bmatrix}$.

The minimization of χ^2 is obtained by the Levenberg-Marquardt algorithm with the modification suggested by Nielsen (1999).

3.3. Inversion Results

To demonstrate the importance of the selected reactions, we present three experiments, where we progressively include more reac-

tions to show the improvements due to the included reactions. In the first experiment, we reexamine the reactions chosen by Canty et al. (2006), which are $OH + HO_2 \rightarrow H_2O + O_2$ and $O + OH \rightarrow O_2 + H$. The second experiment add one more reaction chosen by Siskind et al. (2013), which is $H + O_2 + M \rightarrow HO_2 + M$. In the third experiment, we will propose our solution to the model-observation discrepancy, which is the O_2 absorption cross section at Lyman α (121.57 nm). The fourth experiment is to test the robustness of our inversion results with a constrained model where the observed H_2O and O_3 profiles are imposed.

3.3.1. Experiment I—Canty Et Al.'s Reactions

Canty et al. (2006) adjusted the reaction rates of $OH + HO_2 \rightarrow H_2O + O_2$ (loss of HO_x) and $O + OH \rightarrow O_2 + H$ (HO_x interconversion); see Table 1. Both reactions have very similar Jacobians in the mesosphere and the stratosphere, which implies degeneracy. The a priori uncertainties are $(f_{O+OH} - 1) = (f_{OH+HO_2} - 1) = 15\%$ (Table 2). The cost function χ^2 is minimized if A_{OH+HO_2} is increased by 29% and A_{O+OH} is reduced by 53%, which well exceed their a priori uncertainties. These results are also different from Canty et al.'s (2006) results, where A_{OH+HO_2} is increased by 20% and A_{O+OH} is increased by 4% (relative to the 2011 JPL Data Evaluation).

The resultant OH and HO_2 profiles are shown in Figure 4. There is a significant increase (~50%) in the mesospheric OH, caused by the much slower OH destruction through $O + OH \rightarrow O_2 + H$ after inversion. However, the same reaction leads to an increase in the stratospheric OH. To compensate this stratospheric increase, the HO_x sink reaction $OH + HO_2 \rightarrow H_2O + O_2$ has to be 29% faster. But the resultant OH concentration at 40 km still exceeds the observed value. More seriously, the faster HO_x sink reaction results in a significant decrease of HO_2 at all altitudes, leading to a larger discrepancy between the model and the observation.

As a result of the inversion, there is a slight increase in the simulated H_2O that makes the simulated H_2O profile be more consistent with the observed H_2O profile. However, there is also an increase in the simulated O_3 that moves the simulated O_3 profile further away from the observed O_3 profile.

As a sensitivity test on the choice of reactions having similar Jacobians, we perform another experiment where we replace $O + OH \rightarrow O_2 + H$ by $O + HO_2 \rightarrow HO + O_2$ (not shown), which was another HO_x conversion cycle chosen by Jucks et al. (1998). The improvement in the mesospheric OH is worse because of a more stringent a priori uncertainty $(f_{O+HO_2} - 1) = 5\%$.

3.3.2. Experiment II—Addition of $H + O_2 + M \rightarrow HO_2 + M$

Siskind et al. (2013) adopted a rate coefficient for $H + O_2 + M \rightarrow HO_2 + M$ from Wong and Davis (1974), which was 36% faster than the recommended value in 2011 JPL Data Evaluation in order to increase the mesospheric OH and HO_2 . We add this reaction to Canty et al.'s (2006) selection and perform the inversion, with $(f_{H+O_2+M} - 1) = 30\%$ (Table 2). The Jacobian of this reaction has a singular peak at 76 km (Figure 3d). As a result, the cost function χ^2 is minimized if A_{OH+HO_2} is reduced by 13%, A_{O+OH} is reduced by 31%, and A_{H+O_2+M} is increased by 131%. In this experiment, the change in A_{OH+HO_2} is of opposite sign to that in Experiment I but is within the laboratory uncertainty. In contrast, the a posteriori A_{O+OH} and A_{H+O_2+M} well exceed the a priori uncertainties. A_{H+O_2+M} is more than double the a priori value and is much more than the rate coefficient suggested by Siskind et al. (2013) and Wong and Davis (1974) (Table 1).

The increased kinetic rate coefficient A_{H+O_2+M} help improve the simulated OH and HO_2 above 76 km significantly (Figure 5) by producing more HO_2 and hence OH (through $O + HO_2 \rightarrow O_2 + OH$) above

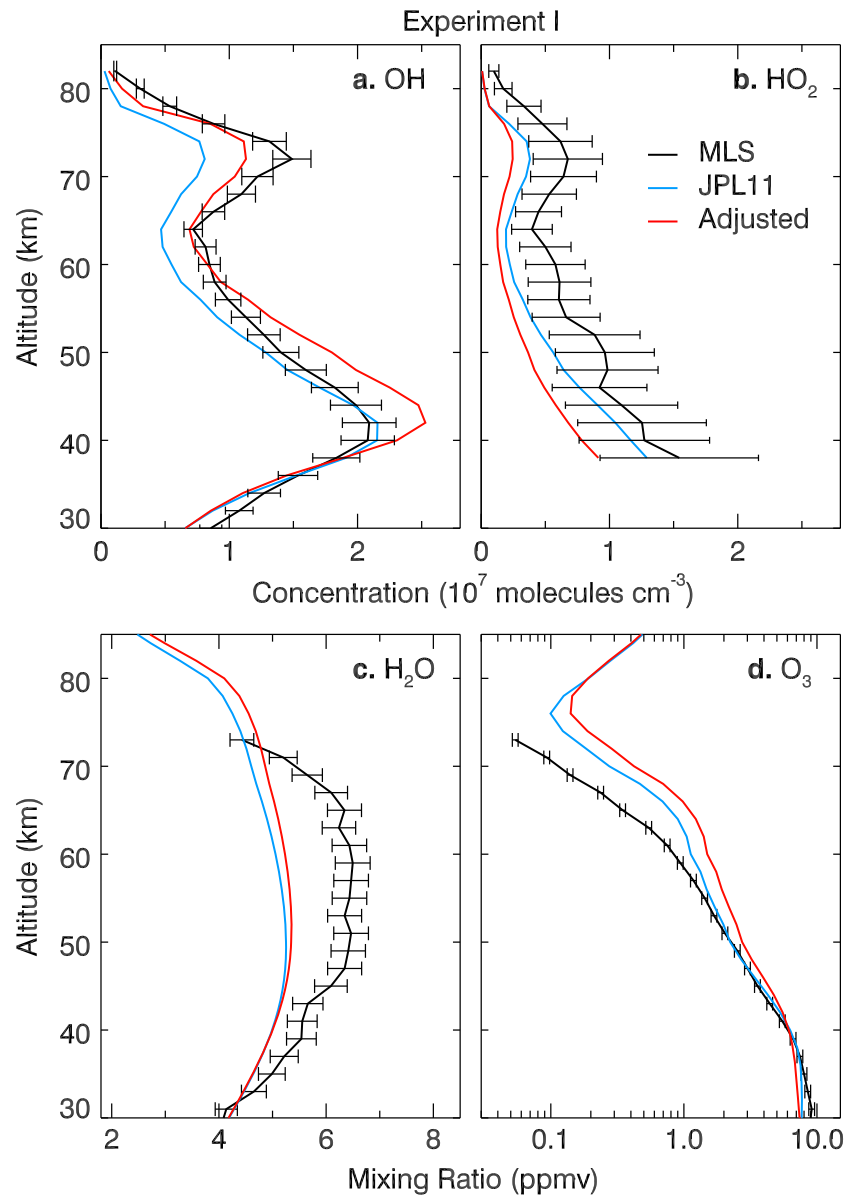


Figure 4. Same as Figure 1 except the simulated OH, HO₂, H₂O, and O₃ profiles after adjusting reaction rate coefficients for O + OH → O₂ + H and OH + HO₂ → H₂O + O₂ are also shown.

72 km. As a result, the reduction in the kinetic rate of O + OH → O₂ + H is less than that in Experiment I. The modified OH profile below 72 km is the same as that in Experiment I, but the HO₂ profile below 72 km is the same as that before the inversion.

The doubling of A_{H+O₂+M} seems to contradict with the laboratory measurements. We shall discuss the important implications of the adjusted A_{H+O₂+M} in section 4.

As in Experiment I, there is an increase in the simulated H₂O, which makes the resultant H₂O profile more consistent with the observation. The simulated O₃, in contrast, remains the same as in a priori profile, except above 76 km, where the adjustment of A_{H+O₂+M} reduces the mesospheric O₃.

3.3.3. Experiment III—O₂ Absorption Cross Section

The improvements of mesospheric OH and HO₂ in Experiments I and II are not satisfactory. Parameters that have been adjusted in previous work are predominantly kinetic rates. An exception is Siskind et al. (2013),

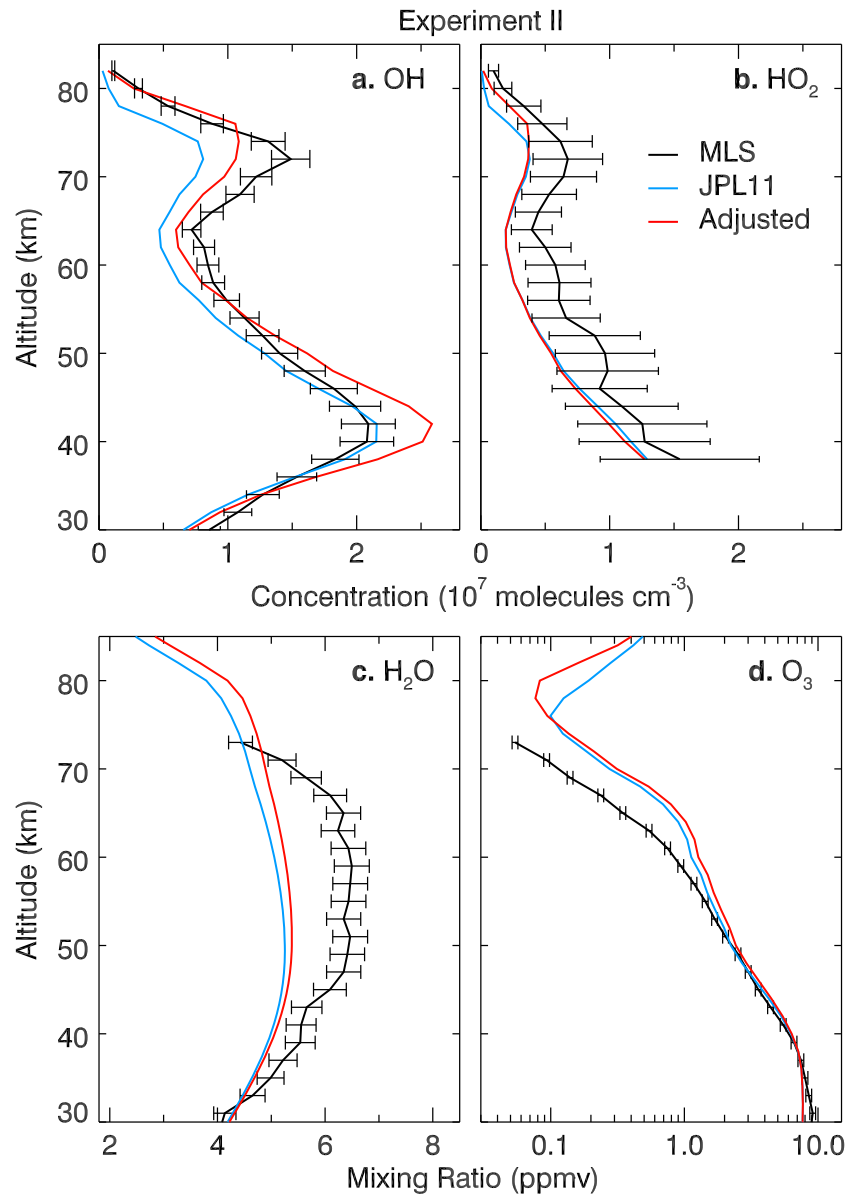


Figure 5. Same as Figure 4 except with adjustments of the reaction rate coefficients for $O + OH \rightarrow O_2 + H$, $OH + HO_2 \rightarrow H_2O + O_2$, and $H + O_2 + M \rightarrow HO_2 + M$.

who also considered the uncertainty in the top-of-atmosphere (TOA) Lyman α intensity, which primarily affects the H_2O photo dissociation through $H_2O + h\nu$ (121.57 nm) \rightarrow H + OH between 65 km and 80 km. We perform an experiment adjusting the Lyman α intensity alone (not shown). The Lyman α intensity would need to be increased by an unrealistic 300% to produce a mesospheric OH concentration comparable to the MLS observation. Therefore, we seek another solution.

The optical depth at Lyman α reaches unity above 80 km due to O_2 absorption (see Figure 3.7 of Liou, 2002). The weaker the O_2 absorption at Lyman α is, the deeper the solar Lyman α can penetrate into the mesosphere, and the stronger response of the H_2O photo dissociation to the 11 year solar variability will be. Thus, besides adjusting the TOA Lyman α intensity as Siskind et al. (2013) did, the H_2O photo dissociation rate at 75 km can also be indirectly adjusted by modifying the O_2 absorption cross section at Lyman α . To demonstrate this effect, we show in Figure 6a the partial derivatives of the OH and HO_2 profiles with respect to the

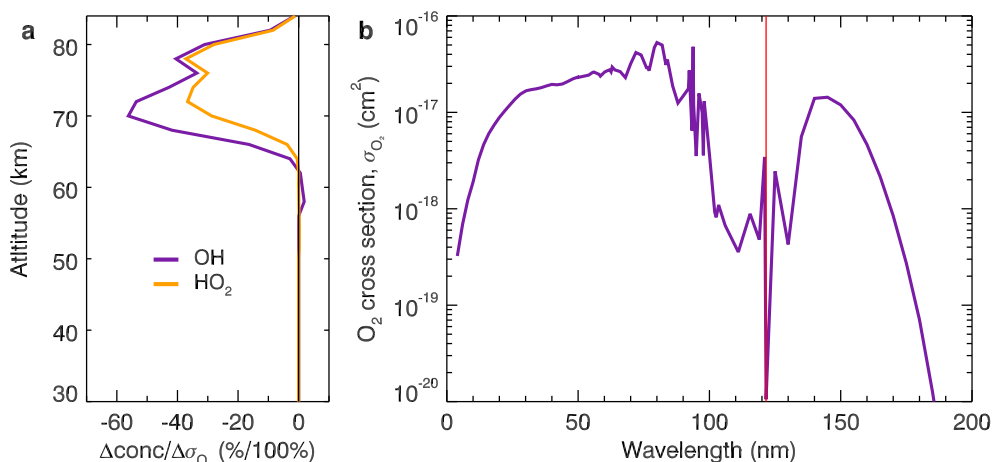


Figure 6. (a) Jacobian of OH (black) and HO₂ (red) with respect to the O₂ photo absorption cross section at Lyman α , in unit of percent change in concentration per 100% change in the O₂ photo absorption cross section (σ_{O_2}). (b) O₂ photo absorption cross section as a function of wavelength, Lyman α (121.57 nm) wavelength is marked with a vertical red line.

O₂ absorption cross section at the Lyman α line, which reveal a broad peak coinciding with the OH and HO₂ mesospheric peak.

Indeed, the O₂ photo absorption cross section at Lyman α is a singular dip, which is 2 orders of magnitude smaller than the continuum at the neighboring wavelengths (Figure 6b) (Liang et al., 2007). This “singular window” in the O₂ absorption cross section allows more Lyman α intensity to penetrate into the lower atmosphere than other FUV flux (Nicolet & Peetermans, 1980). We argue that the singular dip of the O₂ photo absorption cross section at Lyman α is very difficult to be measured accurately in the laboratory and may thus be subject to large uncertainty. We thus include the O₂ absorption cross section at Lyman α as another adjustable model parameter. From 121.52 nm to 121.62 nm, the O₂ cross section monotonically decreases from 1.74×10^{-20} cm² to 0.52×10^{-20} cm² (Lewis et al., 1983), while in the 1-D photochemical model, we adopt an average value of 1.06×10^{-20} cm² at 121.57 nm over this wavelength range.

The temperature dependence of the O₂ absorption cross section may be a source of uncertainty. Lewis et al. (1983) measured the O₂ absorption cross section near Lyman α at a very high resolution (0.01 nm). They showed that the implied column O₂ dissociation rate generally was within 10–15% of previously reported values if the temperature dependence was ignored. Another source of the uncertainty of the O₂ absorption cross section is due to the relatively coarse spectral resolution (0.1 nm) at Lyman α in our 1-D photochemical model, which is not enough to accurately represent the dramatic change up to several orders of magnitude (Figure 6b) (Ogawa, 1968). With the above considerations, we heuristically assume a conservative estimate of an uncertainty of 30% for the O₂ absorption cross section at Lyman α (Table 2).

As a result, the cost function χ^2 is minimized if the O₂ absorption cross section at the Lyman α line is reduced by 54%, A_{OH+HO_2} and A_{O+OH} are both reduced by 15%, and A_{H+O_2+M} is increased by 134%. Note that with the addition of O₂ absorption cross section, the adjustment in A_{O+OH} is now within the measurement uncertainty.

Figure 7 shows the OH and HO₂ profiles after the inversion. The mesospheric OH concentration between 60 and 74 km has significantly increased compared to the previous two experiments, which greatly improves the agreement between the simulated and observed OH mesospheric concentrations. Because the reduction of A_{O+OH} is less than that in Experiment II, the simulated stratospheric OH agrees better with observation. Meanwhile, the simulated mesospheric HO₂ also agrees better with observations.

As in Experiments I and II, there is an increase in the simulated H₂O. The reduction of the O₂ absorption cross section reduces the mesospheric O₃ between 62 km and 76 km and the simulated O₃ profile agrees better with the observed O₃ over this range.

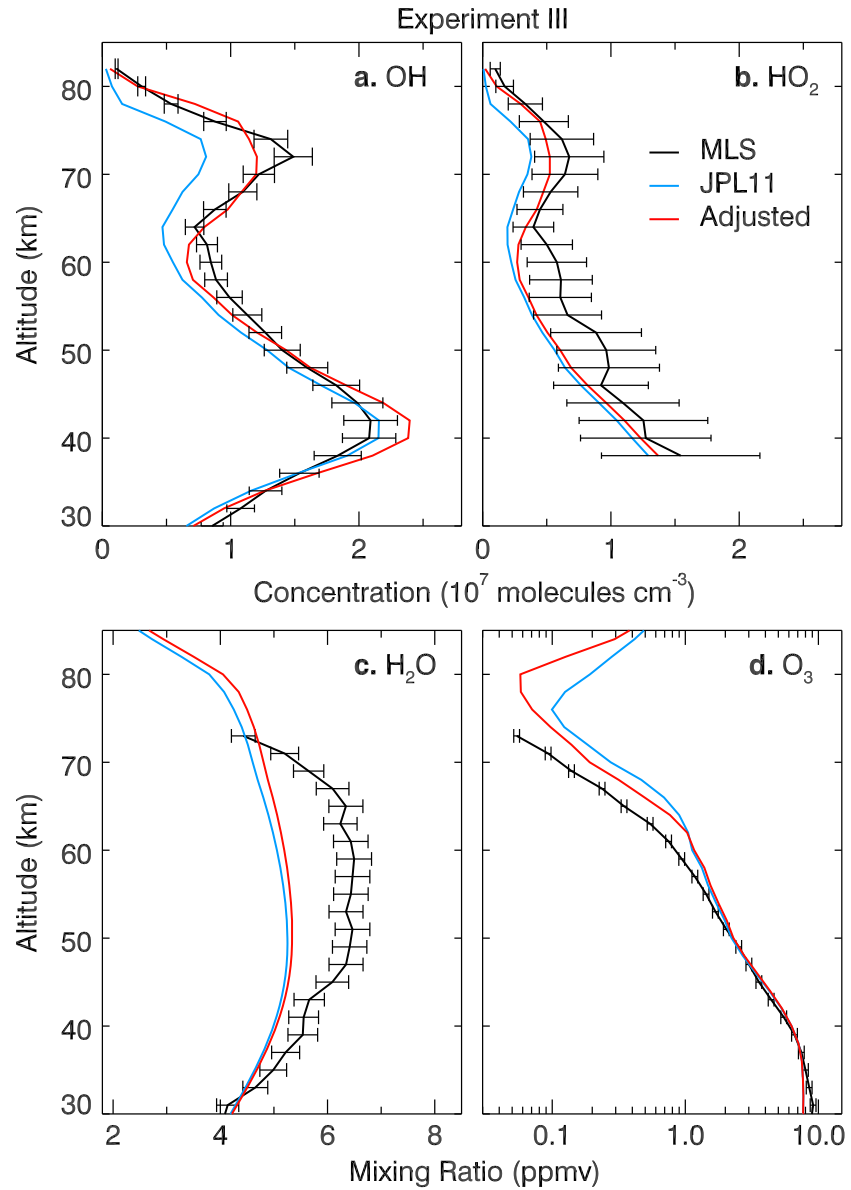


Figure 7. Same as Figure 4 except with adjustments of the reaction rate coefficients for $O + OH \rightarrow O_2 + H$, $OH + HO_2 \rightarrow H_2O + O_2$, $H + O_2 + M \rightarrow HO_2 + M$, and the O_2 absorption cross section at Lyman α .

Again, as a sensitivity test on the choice of reactions having similar Jacobians, we replace $O + OH \rightarrow O_2 + H$ by $O + HO_2 \rightarrow O_2 + OH$ and perform the inversion. In this case, the cost function χ^2 is minimized if the O_2 absorption cross section at the Lyman α line is reduced by 58%, A_{OH+HO_2} is reduced by 30%, A_{O+HO_2} is reduced by 10%, and A_{H+O_2+M} is increased by 173%. Thus, the inversion results are qualitatively consistent with those by adjusting A_{O+OH} .

3.3.4. Experiment IV—Simulations With H₂O and O₃ Constraints

A concern about Experiments I–III is that the modeled H₂O and O₃ profiles are not realistic comparing to the MLS observations (see the discussion in section 2.2 and see Figures 1, 4, 5, and 7). We thus recalculate the model OH and HO₂ profiles by constraining the H₂O and O₃ profiles using the zonally and tropically (25°N–25°S) averaged MLS daytime observation at 30–72 km. The a priori profiles are plotted in Figure 8 (green lines), which are compared with the a priori profiles obtained from the unconstrained simulation (blue lines). After imposing the MLS H₂O and O₃ constraints, the simulated OH and HO₂ concentrations are

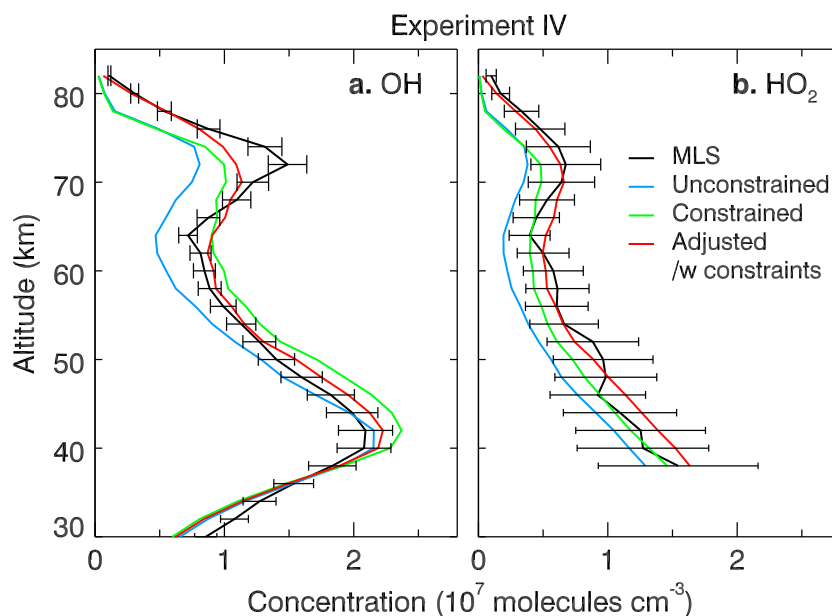


Figure 8. Comparison of the simulated OH and HO₂ profiles (i) before (blue) and after (green) constraining the model H₂O and O₃ profiles with the MLS observations and (ii) before (green) and after (red) the adjustments of the reaction rate coefficients for O + OH → O₂ + H, OH + HO₂ → H₂O + O₂, H + O₂ + M → HO₂ + M, and the O₂ absorption cross section at Lyman α given the MLS H₂O and O₃ constraints.

generally higher between 40 and 72 km than the unconstrained simulation, primarily due to the increased source of OH from the photolysis of H₂O and the recombination of H₂O and O(¹D). Moreover, while the simulated OH is higher than observed below 65 km, it is significantly lower than observed above 65 km, especially at the mesospheric peak, which is consistent with the result of Millán et al. (2015).

With the MLS H₂O and O₃ constraints, the cost function χ^2 is minimized if the O₂ absorption cross section at the Lyman α line is reduced by 34%, $A_{\text{OH}+\text{HO}_2}$ is reduced by 10%, $A_{\text{O}+\text{OH}}$ is increased by 12%, and $A_{\text{H}+\text{O}_2+\text{M}}$ is increased by 310%. The a posteriori OH and HO₂ profiles are shown in Figure 8 (red lines). Three comments are in order.

1. The inferred change in the O₂ absorption cross section at Lyman α is qualitatively consistent with the result obtained from Experiment III. Therefore, the application of the MLS H₂O and O₃ constraints still implies the need for a reexamination of the O₂ absorption cross section at Lyman α.
2. $A_{\text{H}+\text{O}_2+\text{M}}$ is still required to be much larger than the 2011 JPL Data Evaluation after imposing the MLS H₂O and O₃ constraints, again urging for a reexamination of the reaction H + O₂ + M → HO₂ + M.
3. Although the change of $A_{\text{O}+\text{OH}}$ becomes positive after imposing the MLS H₂O and O₃ constraints, the magnitude of the change is well within the experimental uncertainty. Thus, the inferred $A_{\text{O}+\text{OH}}$ is consistent with the 2011 JPL Data Evaluation. The increase in $A_{\text{O}+\text{OH}}$ leads to a decrease the stratospheric OH and an increase the stratospheric HO₂, so that the adjusted stratospheric OH and HO₂ agree better with the observations than in other experiments.

4. Summary and Discussion

We have proposed a systematic approach to estimate model parameters based on high-quality satellite observations. The Bayesian optimal estimation helps quantify model parameter uncertainties and provide guidance to laboratory measurements for key reactions. Such an inversion requires a large number of runs to estimate the model sensitivity with respect to each parameter. A computationally inexpensive 1-D photochemical model is particular useful for such a sensitivity calculation. Since HO_x chemistry in the mesosphere and stratosphere is simple and mainly controlled by several key reactions, the simplification in the transport in the 1-D model has little effect on our conclusions. In this model, all transports including vertical winds and

gravity wave mixing (Grygalashvily et al., 2011) are parameterized using eddy diffusion. The most significant impact on the concentrations of HO_x species from this simplified scheme is the transport of H₂O. We tested the impact of perturbations in the vertical eddy diffusivity to the OH and HO₂ profiles. The largest impact is found in the lower stratospheric HO_x, due to the transport of tropospheric H₂O into the stratosphere at the tropopause which subsequently enhanced the production OH via H₂O + O(¹D) → 2OH. However, the partial derivatives of the OH and HO₂ profiles with respect to changes in the eddy diffusivity is of the order of 10⁵, which is one order of magnitude smaller than the Jacobians of important reaction rate coefficients.

We have used the kinetic rate coefficients in the 2011 JPL Data Evaluation, which may differ from previous evaluations; see the footnotes in Table 1. For example, the 2011 JPL Data Evaluation for the kinetic rate coefficient for O + OH → O₂ + H is 16% higher than that in the 2006 JPL Data Evaluation. Thus, the retrieved rate for O + OH → O₂ + H in this study would be 31% larger than that in JPL 2006 Evaluation. We have considered both the stratospheric and mesospheric peaks in the OH and HO₂ profiles, in contrast to some previous studies, such as Canty et al. (2006), who considered only stratospheric OH and HO₂. In addition to the reactions listed in Table 1, we also tried other combinations of reactions, including some NO_x reactions. Their fittings are worse than the result we have shown above.

The kinetic rate coefficient for H + O₂ + M → HO₂ + M is required to be more than double, while the measurement uncertainty recommended by the 2011 JPL Data Evaluation is only 30%. This is also much larger than the perturbations made to other model parameters. There are two possible explanations. The first one relies on the fact that this reaction is primarily contributing to the production of OH and HO₂ in the mesosphere (Figure 3b). At this altitude, pressure and temperature are extremely low. At 78 km where the Jacobian for this reaction is maximum, atmospheric pressure is only 0.022 hPa. Most of the measurements of this reaction are done at much higher pressure and temperature (Sander et al., 2011, and references therein) and may not be accurate at such a low pressure level, where the characteristic times of odd hydrogen and odd oxygen increase with altitude and the reactions at high altitude may not have reached the steady state. Thus, in view of the large increase in rate constant for the H + O₂ + M inferred from our inversion, we have reexamined the kinetics database for this reaction, similar to that presented in Siskind et al. (2013). The NASA JPL Panel considered 11 laboratory studies of this reaction which used several different techniques over a wide range of pressure and temperature. A large majority of these studies focused on the temperature range relevant to combustion conditions, 298 ≤ T ≤ 1500 K. Only two studies presented data relevant to the middle atmosphere. Both Kurylo (1972) and Wong and Davis (1974) used the flash photolysis-atomic resonance fluorescence technique to measure termolecular rate coefficients below room temperature using several different bath gases. For M = N₂ at 220 K, Kurylo (1972) obtained 8.35 × 10⁻³² cm⁶ molecule⁻² s⁻¹, while Wong and Davis (1974) obtained (8.6 ± 1.6) × 10⁻³² cm⁶ molecule⁻² s⁻¹. The rate coefficient recommended by the NASA Panel for M = N₂ at 220 K is considerably smaller: 6.6 × 10⁻³² cm⁶ molecule⁻² s⁻¹. At 298 K, where there are several additional studies, the average of the k₂₉₈ rate coefficients is also about 25–30% larger than the NASA recommendation. It should be noted that the NASA Panel accepted the recommendation contained in a theoretical paper by Sellevåg et al. (2008) which was aimed at obtaining a suitable fit between two-dimensional master equation calculations and the high-temperature kinetics database for the purposes of combustion studies. Inspection of Figure 4b in Sellevåg et al. (2008) which compares their master equation results with the lab data near room temperature for M = N₂ clearly shows that the theoretical results fall below all the experimental data in the termolecular pressure regime. Therefore, the Sellevåg et al. (2008) values, and implicitly the JPL Data Evaluation, is unsuitable for the pressure and temperature range of interest for the altitude regime considered in the present study. At 170 K in the lower mesospheric region, the rate coefficient calculated using Wong and Davis's (1974) exponential parameterization that is 52% larger than the 2011 JPL Data Evaluation and Siskind et al. (2013) showed that this rate coefficient produced a more realistic HO_x concentration in the lower mesosphere. Therefore, we suggest that a value for the H + O₂ + N₂ termolecular rate coefficient that is 25–50% larger than the JPL Data Evaluation is an appropriate choice. Yet this increase in the rate coefficient is still too small compared to our optimized value.

A second possible explanation, which might help enhance the effective rate constant of H + O₂ → HO₂ under upper stratospheric conditions and which has not been considered in the literature thus far, is the radiative association (Vuitton et al., 2012). In the mesosphere, the limiting factor of the three body reaction is the total concentration of M due to the low pressure. At this level, the radiative association reaction (A + B → AB + hν)

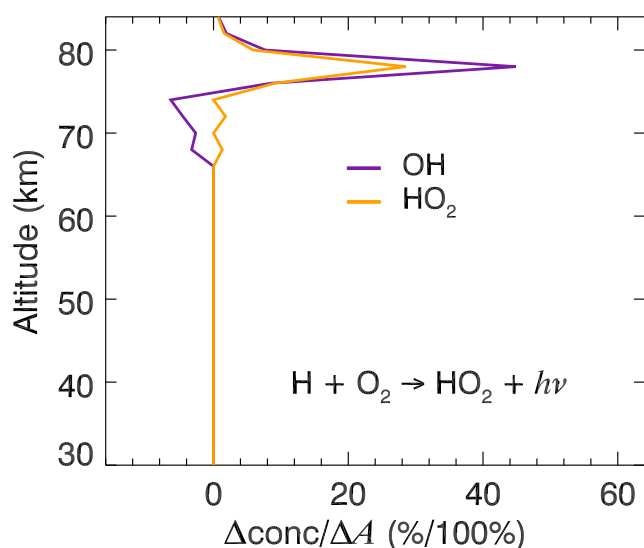


Figure 9. The Jacobians of OH (purple) and HO₂ (orange) with respect to the radiative association reaction $\text{H} + \text{O}_2 \rightarrow \text{HO}_2 + h\nu$ with a nominal reaction rate of $7 \times 10^{-17} \text{ s}^{-1} \text{ cm}^3$.

may have a similar or even higher order of magnitude reaction rate than the three-body reaction ($\text{A} + \text{B} + \text{M} \rightarrow \text{AB} + \text{M}$). The reaction enthalpy, ΔH (298 K), for the radiative association is $-49.2 \text{ kcal mol}^{-1}$, which is much larger than the energy required to populate the low-lying $\tilde{\text{A}}$ electronic state of HO₂ at about $17,200 \text{ cm}^{-1}$ provided that the required electronic curve crossing is sufficiently rapid. This would also require a favorable fluorescence lifetime for the $\tilde{\text{A}}^2\text{A}' \rightarrow \tilde{\text{X}}^2\text{A}''$ transition, which is reasonably strong in absorption. As an estimation, we calculate the reaction rate of $\text{H} + \text{O}_2 + \text{M} \rightarrow \text{HO}_2 + \text{M}$ at 78 km altitude using the low-pressure limit:

$$k = k_0^{300} \left(\frac{T}{300} \right)^{-n} [M] \quad (9)$$

where $T = 191.6 \text{ K}$, $[M] = 6.32 \times 10^{14} \text{ cm}^{-3}$. In the JPL 2011 evaluation, $k_0^{300} = 4.4 \times 10^{-32} \text{ s}^{-1} \text{ cm}^6$, $n = 1.3$. To compensate for the 134% increase in the three body reaction rate for $\text{H} + \text{O}_2 + \text{M} \rightarrow \text{HO}_2 + \text{M}$, a radiative association reaction rate coefficient of $\sim 7 \times 10^{-17} \text{ s}^{-1} \text{ cm}^3$ for $\text{H} + \text{O}_2 \rightarrow \text{HO}_2 + h\nu$ is needed. While the radiative association reaction rates have never been measured, Vuitton et al. (2012) calculated several

radical-molecule reaction rates theoretically using transition state theory. They found that the contribution of the photo association reaction in a two-heavy-atom radical-radical reaction rate coefficient is in the order of $1.0 \times 10^{-17} \text{ s}^{-1} \text{ cm}^3$. As a test, this reaction is added to our 1-D model with a nominal reaction rate of $7 \times 10^{-17} \text{ cm}^3 \text{ s}^{-1}$. The partial derivatives of OH and HO₂ with respect to this new reaction exhibit the same sharp peaks in the mesosphere compared with those of $\text{H} + \text{O}_2 + \text{M} \rightarrow \text{HO}_2 + \text{M}$ (Figure 9). The values of their partial derivatives also have the same order of magnitude as those of $\text{H} + \text{O}_2 + \text{M} \rightarrow \text{HO}_2 + \text{M}$.

The method proposed in this study is not limited to studying HO_x chemistry. We choose to use the stratospheric and mesospheric HO_x mean profiles because they are very well measured by MLS and are mainly controlled by simple chemistry. The same method could be applied to solve other model-observation discrepancy problems.

Acknowledgments

We thank P. Wennberg, R. L. Shia, S. Newman, and P. Kopparla for helpful comments. We acknowledge the support of the NASA Aura Science Team. S. W., Q. Z., and Y. L. Y. acknowledge partial support by NASA's LWS Program grant NNX16AK63G. K. F. L. was supported partly by the Jack Eddy Fellowship managed by the University Corporation for Atmospheric Research and partly by the NASA grant NNX14AR40G. We thank the two anonymous reviewers, whose comments significantly improved this manuscript. Additional support was provided by the NASA Upper Atmosphere Research and Tropospheric Chemistry Programs. MLS data are available at https://mls.jpl.nasa.gov/products/oh_product.php.

References

- Allen, M., Yung, Y. L., & Waters, J. W. (1981). Vertical transport and photochemistry in the terrestrial mesosphere and lower thermosphere (50–120 km). *Journal of Geophysical Research*, *86*, 3617–3627. <https://doi.org/10.1029/JA086iA05p03617>
- Anderson, J. G. (1971). Rocket measurement of OH in the mesosphere. *Journal of Geophysical Research*, *76*, 7820–7824. <https://doi.org/10.1029/JA076i031p07820>
- Brasseur, G. P., & Solomon, S. (2005). *Aeronomy of the Middle Atmosphere: Chemistry and Physics of the Stratosphere and Mesosphere* (3rd ed.). (pp. 646). Dordrecht, Netherlands: Springer.
- Burnett, C. R., & Burnett, E. B. (1981). Spectroscopic measurements of the vertical column abundance of hydroxyl (OH) in the Earth's atmosphere. *Journal of Geophysical Research: Oceans*, *86*, 5185–5202. <https://doi.org/10.1029/JC086iC06p05185>
- Cageao, R. P., Blavier, J. F., McGuire, J. P., Jiang, Y., Nemtchinov, V., Mills, F. P., & Sander, S. P. (2001). High-resolution Fourier-transform ultraviolet-visible spectrometer for the measurement of atmospheric trace species: Application to OH. *Applied Optics*, *40*, 2024–2030. <https://doi.org/10.1364/AO.40.002024>
- Canty, T., & Minschwaner, K. (2002). Seasonal and solar cycle variability of OH in the middle atmosphere. *Journal of Geophysical Research: Atmospheres*, *107*(D24), 4737. <https://doi.org/10.1029/2002JD002278>
- Canty, T., Pickett, H. M., Salawitch, R. J., Jucks, K. W., Traub, W. A., & Waters, J. W. (2006). Stratospheric and mesospheric HO_x: Results from aura MLS and FIRS-2. *Geophysical Research Letters*, *33*, L12802. <https://doi.org/10.1029/2006GL025964>
- Conway, R. R., Stevens, M. H., Brown, C. M., Cardon, J. G., Zasadil, S. E., & Mount, G. H. (1999). Middle Atmosphere High Resolution Spectrograph Investigation. *Journal of Geophysical Research: Atmospheres*, *104*, 16,327–16,348. <https://doi.org/10.1029/1998JD100036>
- Conway, R. R., Summers, M. E., Stevens, M. H., Cardon, J. G., Preusse, P., & Offermann, D. (2000). Satellite observations of upper stratospheric and mesospheric OH: The HO_x dilemma. *Geophysical Research Letters*, *27*, 2613–2616. <https://doi.org/10.1029/2000GL011698>
- DeMore, W. B., Golden, D. M., Hampson, R. F., Howard, C. J., Kurylo, M. J., Molina, M. J., ... Sander, S. P. (1994). *JPL Publication 94-26*. Pasadena, CA: Jet Propulsion Laboratory, California Institute of Technology.
- DeMore, W. B., Sander, S. P., Golden, D. M., Hampson, R. F., Kurylo, M. J., Howard, C. J., ... Molina, M. J. (1997). Chemical kinetics and photochemical data for use in stratospheric modeling, evaluation no. 12, JPL Publication 97-4, Jet Propulsion Laboratory, Pasadena, CA. [Available at <http://jpldataeval.jpl.nasa.gov>]
- Englert, C. R., Schimpf, B., Birk, M., Schreier, F., Krocka, M., Nitsche, R. G., ... Summers, M. E. (2000). The 2.5 THz heterodyne spectrometer THOMAS: Measurement of OH in the middle atmosphere and comparison with photochemical model results. *Journal of Geophysical Research: Atmospheres*, *105*, 22,211–22,223. <https://doi.org/10.1029/2000JD900305>

- Englert, C. R., Stevens, M. H., Siskind, D. E., Harlander, J. M., Roesler, F. L., Pickett, H. M., ... Kochenash, A. J. (2008). First results from the Spatial Heterodyne Imager for Mesospheric Radicals (SHIMMER): Diurnal variation of mesospheric hydroxyl. *Geophysical Research Letters*, *35*, L19813. <https://doi.org/10.1029/2008GL035420>
- Grygalashvily, M., Becker, E., & Sonnemann, G. R. (2011). Wave mixing effects on minor chemical constituents in the MLT region: Results from a global CTM driven by high-resolution dynamics. *Journal of Geophysical Research: Atmospheres*, *116*, D18302. <https://doi.org/10.1029/2010JD015518>
- Heaps, W. S., & McGee, T. J. (1985). Progress in stratospheric hydroxyl measurement by balloon-borne LIDAR. *Journal of Geophysical Research: Atmospheres*, *90*, 7913–7921. <https://doi.org/10.1029/JD090iD05p07913>
- Iwagami, N., Inomata, S., Murata, I., & Ogawa, T. (1995). Doppler detection of hydroxyl column abundance in the middle atmosphere. *Journal of Atmospheric Chemistry*, *20*, 1–15. <https://doi.org/10.1007/BF01099915>
- Jucks, K. W., Johnson, D. G., Chance, K. V., Traub, W. A., Margitan, J. J., Osterman, G. B., ... Sasano, Y. (1998). Observations of OH, HO₂, H₂O, and O₃ in the upper stratosphere: Implications for HO_x photochemistry. *Geophysical Research Letters*, *25*, 3935–3938. <https://doi.org/10.1029/1998GL900009>
- Kendall, D. J. W., & Clark, T. A. (1980). Stratospheric observation of far IR pure rotational lines of hydroxyl. *Nature*, *283*, 57–58. <https://doi.org/10.1038/283057a0>
- Kurylo, M. J. (1972). Absolute rate constants for reaction H + O₂ + M → HO₂ + M over temperature range 203–404 K. *The Journal of Physical Chemistry*, *76*, 3518–3526. <https://doi.org/10.1021/j100668a002>
- Lean, J. (2000). Evolution of the Sun's spectral irradiance since the Maunder Minimum. *Geophysical Research Letters*, *27*, 2425–2428. <https://doi.org/10.1029/2000GL000043>
- Lewis, B. R., Vardavas, I. M., & Carver, J. H. (1983). The aeronomic dissociation of water-vapor by solar-H Lyman alpha-radiation. *Journal of Geophysical Research: Space Physics*, *88*, 4935–4940. <https://doi.org/10.1029/JA088iA06p04935>
- Liang, M.-C., Blake, G. A., Lewis, B. R., & Yung, Y. L. (2007). Oxygen isotopic composition of carbon dioxide in the middle atmosphere. *Proceedings of the National Academy of Sciences of the United States of America*, *104*, 21–25. <https://doi.org/10.1073/pnas.0610009104>
- Liou, K. N. (2002). *An Introduction to Atmospheric Radiation* (2nd ed., pp. 583). San Diego, CA: Academic Press.
- Livesey, N. J., Read, W. G., Wagner, P. A., Froidevaux, L., Lambert, A., Manney, G. L., ... Martinez, E. (2015). *Version 4.2x Level 2 Data Quality and Description Document*. Pasadena, CA: Jet Propulsion Laboratory.
- Millán, L., Wang, S., Livesey, N. J., Kinnison, D., Sagawa, H., & Kasai, Y. (2015). Stratospheric and mesospheric HO₂ observations from the Aura Microwave Limb Sounder. *Atmospheric Chemistry and Physics*, *15*, 2889–2902. <https://doi.org/10.5194/acp-15-2889-2015>
- Nicolet, M., & Peetermans, W. (1980). Atmospheric absorption in the O₂ schumann-runge band spectral range and photo-dissociation rates in the stratosphere and mesosphere. *Planetary and Space Science*, *28*, 85–103. [https://doi.org/10.1016/0032-0633\(80\)90106-3](https://doi.org/10.1016/0032-0633(80)90106-3)
- Nielsen, H. B. (1999). Damping parameter in Marquardt's method (Tech. Rep., IMM-REP-1999-1905). Informatics and Mathematical Modelling, Technical University of Denmark.
- Ogawa, M. (1968). Absorption coefficients of O₂ at the Lyman-alpha line and its vicinity. *Journal of Geophysical Research*, *73*, 6759–6763. <https://doi.org/10.1029/JA073i021p06759>
- Park, J. H., & Carli, B. (1991). Spectroscopic measurement of HO₂, H₂O₂ and OH in the stratosphere. *Journal of Geophysical Research: Atmospheres*, *96*, 22,535–22,541. <https://doi.org/10.1029/91JD02327>
- Pickett, H. M. (2006). Microwave Limb Sounder THz module on Aura. *IEEE Transactions on Geoscience and Remote Sensing*, *44*, 1122–1130. <https://doi.org/10.1109/TGRS.2005.862667>
- Pickett, H. M., Drouin, B. J., Canty, T., Kovalenko, L. J., Salawitch, R. J., Livesey, N. J., ... Traub, W. A. (2006). Validation of Aura MLS HO_x measurements with remote-sensing balloon instruments. *Geophysical Research Letters*, *33*, L01808. <https://doi.org/10.1029/2005GL024048>
- Pickett, H. M., Drouin, B. J., Canty, T., Salawitch, R. J., Fuller, R. A., Perun, V. S., ... Minschwaner, K. (2008). Validation of Aura Microwave Limb Sounder OH and HO₂ measurements. *Journal of Geophysical Research: Atmospheres*, *113*, D16530. <https://doi.org/10.1029/2007JD008775>
- Pickett, H. M., & Peterson, D. B. (1993). Stratospheric OH measurements with a far-infrared limb observing spectrometer. *Journal of Geophysical Research: Atmospheres*, *98*, 20,507–20,515. <https://doi.org/10.1029/93JD02183>
- Rodgers, C. D. (2000). *Inverse Methods for Atmospheric Sounding: Theory and Practice* (240 pp.). Singapore: World Scientific.
- Rožanov, E., Egorova, T., Schmutz, W., & Peter, T. (2006). Simulation of the stratospheric ozone and temperature response to the solar irradiance variability during sun rotation cycle. *Journal of Atmospheric and Solar-Terrestrial Physics*, *68*, 2203–2213. <https://doi.org/10.1016/j.jastp.2006.09.004>
- Sander, S. P., Finlayson-Pitts, B. J., Friedl, R. R., Golden, D. M., Huie, R. E., Kolb, C. E., ... Ravishankara, A. R. (2002). Chemical kinetics and photochemical data for use in atmospheric studies, Evaluation No. 14, JPL Publication 02-25, Jet Propulsion Laboratory, Pasadena, CA. [Available at <http://jpldataeval.jpl.nasa.gov/>]
- Sander, S. P., Finlayson-Pitts, B. J., Friedl, R. R., Golden, D. M., Huie, R. E., Keller-Rudek, H., ... Wine, P. H. (2006). Chemical kinetics and photochemical data for use in atmospheric studies, Evaluation No. 15, JPL Publication 06-2, Jet Propulsion Laboratory, Pasadena, CA. [Available at <http://jpldataeval.jpl.nasa.gov/>]
- Sander, S. P., Abbatt, J., Barker, J. R., Burkholder, J. B., Friedl, R. R., Golden, D. M., ... Wine, P. H. (2011). Chemical kinetics and photochemical data for use in atmospheric studies, (Evaluation No. 17, p. 684). JPL Publication 10-6, Jet Propulsion Laboratory, Pasadena, CA. [Available at <http://jpldataeval.jpl.nasa.gov/>]
- Sellevåg, S. R., Georgievskii, Y., & Miller, J. A. (2008). The temperature and pressure dependence of the reactions H + O₂ (+ M) → HO₂ (+ M) and H + OH (+ M) → H₂O (+ M). *The Journal of Physical Chemistry. A*, *112*, 5085–5095. <https://doi.org/10.1021/jp11800z>
- Shapiro, A. V., Rožanov, E., Shapiro, A. I., Wang, S., Egorova, T., Schmutz, W., & Peter, T. (2012). Signature of the 27-day solar rotation cycle in mesospheric OH and H₂O observed by the Aura Microwave Limb Sounder. *Atmospheric Chemistry and Physics*, *12*, 3181–3188. <https://doi.org/10.5194/acp-12-3181-2012>
- Siskind, D. E., Stevens, M. H., Englert, C. R., & Mlynczak, M. G. (2013). Comparison of a photochemical model with observations of mesospheric hydroxyl and ozone. *Journal of Geophysical Research*, *118*, 195–207. <https://doi.org/10.1029/2012JD017971>
- Summers, M. E., Conway, R. R., Siskind, D. E., Stevens, M. H., Offermann, D., Riese, M., ... Russell, J. M. (1997). Implications of satellite OH observations for middle atmospheric H₂O and ozone. *Science*, *277*, 1967–1970. <https://doi.org/10.1126/science.277.5334.1967>
- Traub, W. A., Johnson, D. G., & Chance, K. V. (1990). Stratospheric hydroperoxyl measurements. *Science*, *247*, 446–449. <https://doi.org/10.1126/science.247.4941.446>
- Vuitton, V., Yelle, R. V., Lavvas, P., & Klippenstein, S. J. (2012). Rapid association reactions at low pressure: Impact on the formation of hydrocarbons on Titan. *The Astrophysical Journal*, *744*, 11. <https://doi.org/10.1088/0004-637x/744/1/11>

- Wang, S., Zhang, Q., Millán, L., Li, K. F., Yung, Y. L., Sander, S. P., ... Santee, M. L. (2015). First evidence of middle atmospheric HO₂ response to 27 day solar cycles from satellite observations. *Geophysical Research Letters*, *42*, 10,004–10,009. <https://doi.org/10.1002/2015GL065237>
- Waters, J. W., Froidevaux, L., Harwood, R. S., Jarnot, R. F., Pickett, H. M., Read, W. G., ... Walch, M. J. (2006). The Earth Observing System Microwave Limb Sounder (EOS MLS) on the Aura satellite. *IEEE Transactions on Geoscience and Remote*, *44*, 1075–1092. <https://doi.org/10.1109/TGRS.2006.873771>
- Wong, W., & Davis, D. D. (1974). Flash photolysis-resonance fluorescence study of reaction of atomic-hydrogen with molecular-oxygen $H + O_2 + M \rightarrow HO_2 + M$. *International Journal of Chemical Kinetics*, *6*, 401–416. <https://doi.org/10.1002/kin.550060310>

**Resolving Model-Observation Discrepancy in the Mesospheric
and Stratospheric HO_x Chemistry**

King-Fai Li^{1,2}, Qiong Zhang³, Shuhui Wang⁴, Stanley P. Sander⁵, and Yuk L. Yung³

¹Department of Applied Mathematics, University of Washington, Seattle, WA, USA

²Department of Environmental Sciences, University of California, Riverside, CA, USA

³Division of Geological and Planetary Sciences, California Institute of Technology, Pasadena, CA, USA

⁴Joint Institute for Regional Earth System Science and Engineering, University of California, Los Angeles, CA, USA

⁵Jet Propulsion Laboratory, California Institute of Technology, Pasadena, CA, USA

Text S1

Complete photolytic and chemical reaction list with Reaction ID

A. Photolytic reactions

- | | |
|--|---|
| 1) $O_2 + h\nu \rightarrow 2O$ | 19) $NO_3 + h\nu \rightarrow NO + O_2$ |
| 2) $O_2 + h\nu \rightarrow O + O(^1D)$ | 20) $N_2O + h\nu \rightarrow N_2 + O(^1D)$ |
| 3) $O_3 + h\nu \rightarrow O_2 + O$ | 21) $N_2O_5 + h\nu \rightarrow NO_2 + NO_3$ |
| 4) $O_3 + h\nu \rightarrow O_2(^1\Delta) + O(^1D)$ | 22) $N_2O_5 + h\nu \rightarrow NO + NO_3 + O$ |
| 5) $O_3 + h\nu \rightarrow O_2 + O(^1D)$ | 23) $HNO_3 + h\nu \rightarrow NO_2 + OH$ |
| 6) $O_3 + h\nu \rightarrow O_2(^1\Delta) + O$ | 24) $HO_2NO_2 + h\nu \rightarrow HO_2 + NO_2$ |
| 7) $O_3 + h\nu \rightarrow 3O$ | 25) $HO_2NO_2 + h\nu \rightarrow OH + NO_3$ |
| 8) $H_2 + h\nu \rightarrow 2H$ | 26) $CH_4 + h\nu \rightarrow CH_3 + H$ |
| 9) $OH + h\nu \rightarrow O + H$ | 27) $CO_2 + h\nu \rightarrow CO + O$ |
| 10) $HO_2 + h\nu \rightarrow OH + O$ | 28) $CO_2 + h\nu \rightarrow CO + O(^1D)$ |
| 11) $H_2O + h\nu \rightarrow H + OH$ | 29) $HCO + h\nu \rightarrow H + CO$ |
| 12) $H_2O + h\nu \rightarrow H_2 + O(^1D)$ | 30) $H_2CO + h\nu \rightarrow 2H + CO$ |
| 13) $H_2O + h\nu \rightarrow 2H + O$ | 31) $H_2CO + h\nu \rightarrow HCO + H$ |
| 14) $H_2O_2 + h\nu \rightarrow 2OH$ | 32) $H_2CO + h\nu \rightarrow H_2 + CO$ |
| 15) $N_2 + h\nu \rightarrow 2N$ | 33) $CH_3O_2 + h\nu \rightarrow CH_3 + O_2$ |
| 16) $NO + h\nu \rightarrow N + O$ | 34) $CH_3OOH + h\nu \rightarrow CH_3O + OH$ |
| 17) $NO_2 + h\nu \rightarrow NO + O$ | |
| 18) $NO_3 + h\nu \rightarrow NO_2 + O$ | |

B. Bi-/Ter-molecular reactions

- 52) $2\text{O} + \text{M} \rightarrow \text{O}_2 + \text{M}$
 53) $2\text{O} + \text{O}_2 \rightarrow \text{O}_3 + \text{O}$
 54) $\text{O} + 2\text{O}_2 \rightarrow \text{O}_3 + \text{O}_2$
 55) $\text{O} + \text{O}_2 + \text{N}_2 \rightarrow \text{O}_3 + \text{N}_2$
 56) $\text{O} + \text{O}_2 + \text{CO} \rightarrow \text{O}_3 + \text{CO}$
 57) $\text{O} + \text{O}_2 + \text{CO}_2 \rightarrow \text{O}_3 + \text{CO}_2$
 58) $\text{O} + \text{O}_2 + \text{M} \rightarrow \text{O}_3 + \text{M}$
 59) $\text{O} + \text{O}_3 \rightarrow 2\text{O}_2$
 60) $\text{O} + \text{H} + \text{M} \rightarrow \text{OH} + \text{M}$
 61) $\text{O} + \text{H}_2 \rightarrow \text{OH} + \text{H}$
 62) $\text{O} + \text{OH} \rightarrow \text{O}_2 + \text{H}$
 63) $\text{O} + \text{HO}_2 \rightarrow \text{OH} + \text{O}_2$
 64) $\text{O} + \text{HO}_2 \rightarrow \text{OH} + \text{O}_2(^1\Delta)$
 65) $\text{O} + \text{H}_2\text{O}_2 \rightarrow \text{OH} + \text{HO}_2$
 66) $\text{O} + \text{NO} + \text{M} \rightarrow \text{NO}_2 + \text{M}$
 67) $\text{O} + \text{NO}_2 \rightarrow \text{NO} + \text{O}_2$
 68) $\text{O} + \text{NO}_2 + \text{M} \rightarrow \text{NO}_3 + \text{M}$
 69) $\text{O} + \text{NO}_3 \rightarrow \text{O}_2 + \text{NO}_2$
 70) $\text{O} + \text{N}_2\text{O}_5 \rightarrow 2\text{NO}_2 + \text{O}_2$
 71) $\text{O} + \text{HNO}_3 \rightarrow \text{OH} + \text{NO}_3$
 72) $\text{O} + \text{HO}_2\text{NO}_2 \rightarrow \text{OH} + \text{NO}_2 + \text{O}_2$
 73) $\text{O} + \text{CH}_3 \rightarrow \text{H}_2\text{CO} + \text{H}$
 74) $\text{O} + \text{CH}_3 \rightarrow \text{CO} + \text{H}_2 + \text{H}$
 75) $\text{O} + \text{CH}_4 \rightarrow \text{CH}_3 + \text{OH}$
 76) $\text{O} + \text{CO} + \text{M} \rightarrow \text{CO}_2 + \text{M}$
 77) $\text{O} + 2\text{CO} \rightarrow \text{CO}_2 + \text{CO}$
 78) $2\text{O} + \text{CO} \rightarrow \text{CO}_2 + \text{O}$
 79) $\text{O} + \text{HCO} \rightarrow \text{H} + \text{CO}_2$
 80) $\text{O} + \text{HCO} \rightarrow \text{OH} + \text{CO}$
 81) $\text{O} + \text{H}_2\text{CO} \rightarrow \text{OH} + \text{HCO}$
 82) $\text{O} + \text{CH}_3\text{O} \rightarrow \text{H}_2\text{CO} + \text{OH}$
 83) $\text{O} + \text{CH}_3\text{O} \rightarrow \text{CH}_3 + \text{O}_2$
 84) $\text{O} + \text{CH}_3\text{O}_2 \rightarrow \text{H}_2\text{CO} + \text{HO}_2$
 85) $\text{O}(^1D) + \text{O}_2 \rightarrow \text{O} + \text{O}_2$
 86) $\text{O}(^1D) + \text{N}_2 \rightarrow \text{O} + \text{N}_2$
 87) $\text{O}(^1D) + \text{CO}_2 \rightarrow \text{O} + \text{CO}_2$
 88) $\text{O}(^1D) \rightarrow \text{O}$
 89) $\text{O}(^1D) + \text{O}_3 \rightarrow 2\text{O}_2$
 90) $\text{O}(^1D) + \text{O}_3 \rightarrow 2\text{O} + \text{O}_2$
 91) $\text{O}(^1D) + \text{H}_2 \rightarrow \text{H} + \text{OH}$
 92) $\text{O}(^1D) + \text{H}_2\text{O} \rightarrow 2\text{OH}$
 93) $\text{O}(^1D) + \text{N}_2 + \text{M} \rightarrow \text{N}_2\text{O} + \text{M}$
 94) $\text{O}(^1D) + \text{N}_2\text{O} \rightarrow 2\text{NO}$
 95) $\text{O}(^1D) + \text{N}_2\text{O} \rightarrow \text{N}_2 + \text{O}_2$
 96) $\text{O}(^1D) + \text{CH}_4 \rightarrow \text{CH}_3 + \text{OH}$
 97) $\text{O}(^1D) + \text{CH}_4 \rightarrow \text{CH}_3\text{O} + \text{H}$
 98) $\text{O}(^1D) + \text{CH}_4 \rightarrow \text{H}_2\text{CO} + \text{H}_2$
 99) $\text{O}_2(^1\Delta) + \text{O} \rightarrow \text{O}_2 + \text{O}$
 100) $\text{O}_2(^1\Delta) + \text{O}_2 \rightarrow 2\text{O}_2$
 101) $\text{O}_2(^1\Delta) + \text{H}_2\text{O} \rightarrow \text{O}_2 + \text{H}_2\text{O}$
 102) $\text{O}_2(^1\Delta) + \text{N}_2 \rightarrow \text{O}_2 + \text{N}_2$
 103) $\text{O}_2(^1\Delta) + \text{CO} \rightarrow \text{O}_2 + \text{CO}$
 104) $\text{O}_2(^1\Delta) + \text{CO}_2 \rightarrow \text{O}_2 + \text{CO}_2$
 105) $\text{O}_2(^1\Delta) + \text{U} \rightarrow \text{O}_2$
 106) $\text{O}_2(^1\Delta) + \text{O}_3 \rightarrow 2\text{O}_2 + \text{O}$
 107) $\text{O}_2(^1\Delta) + \text{N} \rightarrow \text{NO} + \text{O}$
 108) $\text{O}_3 + \text{NO} \rightarrow \text{NO}_2 + \text{O}_2$
 109) $\text{O}_3 + \text{NO}_2 \rightarrow \text{NO}_3 + \text{O}_2$
 110) $\text{H} + \text{O}_2 + \text{M} \rightarrow \text{HO}_2 + \text{M}$
 111) $\text{H} + \text{O}_3 \rightarrow \text{OH} + \text{O}_2$
 112) $2\text{H} + \text{M} \rightarrow \text{H}_2 + \text{M}$
 113) $\text{H} + \text{OH} + \text{N}_2 \rightarrow \text{H}_2\text{O} + \text{N}_2$
 114) $\text{H} + \text{OH} + \text{CO}_2 \rightarrow \text{H}_2\text{O} + \text{CO}_2$
 115) $\text{H} + \text{HO}_2 \rightarrow 2\text{OH}$
 116) $\text{H} + \text{HO}_2 \rightarrow \text{H}_2 + \text{O}_2$
 117) $\text{H} + \text{HO}_2 \rightarrow \text{H}_2 + \text{O}_2(^1\Delta)$
 118) $\text{H} + \text{HO}_2 \rightarrow \text{H}_2\text{O} + \text{O}$
 119) $\text{H} + \text{NO}_2 \rightarrow \text{OH} + \text{NO}$
 120) $\text{H} + \text{NO}_3 \rightarrow \text{OH} + \text{NO}_2$
 121) $\text{H} + \text{CH}_3 + \text{M} \rightarrow \text{CH}_4 + \text{M}$
 122) $\text{H} + \text{CH}_4 \rightarrow \text{CH}_3 + \text{H}_2$
 123) $\text{H} + \text{CO} + \text{M} \rightarrow \text{HCO} + \text{M}$
 124) $\text{H} + \text{HCO} \rightarrow \text{H}_2 + \text{CO}$
 125) $\text{H} + \text{H}_2\text{CO} \rightarrow \text{H}_2 + \text{HCO}$
 126) $\text{H} + \text{CH}_3\text{O} \rightarrow \text{H}_2\text{CO} + \text{H}_2$
 127) $\text{H} + \text{CH}_3\text{O} \rightarrow \text{OH} + \text{CH}_3$
 128) $\text{H} + \text{CH}_3\text{O}_2 \rightarrow \text{CH}_4 + \text{O}_2$
 129) $\text{H} + \text{CH}_3\text{O}_2 \rightarrow \text{H}_2\text{O} + \text{H}_2\text{CO}$
 130) $\text{OH} + \text{O}_3 \rightarrow \text{HO}_2 + \text{O}_2$
 131) $\text{OH} + \text{O}_3 \rightarrow \text{HO}_2 + \text{O}_2(^1\Delta)$
 132) $\text{OH} + \text{H}_2 \rightarrow \text{H}_2\text{O} + \text{H}$
 133) $2\text{OH} \rightarrow \text{H}_2\text{O} + \text{O}$
 134) $2\text{OH} + \text{M} \rightarrow \text{H}_2\text{O}_2 + \text{M}$
 135) $\text{OH} + \text{HO}_2 \rightarrow \text{H}_2\text{O} + \text{O}_2$
 136) $\text{OH} + \text{HO}_2 \rightarrow \text{H}_2\text{O} + \text{O}_2(^1\Delta)$
 137) $\text{OH} + \text{H}_2\text{O}_2 \rightarrow \text{H}_2\text{O} + \text{HO}_2$
 138) $\text{OH} + \text{NO}_2 + \text{M} \rightarrow \text{HNO}_3 + \text{M}$
 139) $\text{OH} + \text{NO}_3 \rightarrow \text{HO}_2 + \text{NO}_2$

- 140) $\text{OH} + \text{HNO}_3 \rightarrow \text{NO}_3 + \text{H}_2\text{O}$
 141) $\text{OH} + \text{HO}_2\text{NO}_2 \rightarrow \text{H}_2\text{O} + \text{NO}_2 + \text{O}_2$
 142) $\text{OH} + \text{CH}_3 \rightarrow \text{H}_2\text{CO} + \text{H}_2$
 143) $\text{OH} + \text{CH}_3 \rightarrow \text{CH}_3\text{O} + \text{H}$
 144) $\text{OH} + \text{CH}_3 \rightarrow \text{CO} + 2\text{H}_2$
 145) $\text{OH} + \text{CH}_4 \rightarrow \text{CH}_3 + \text{H}_2\text{O}$
 146) $\text{OH} + \text{CO} \rightarrow \text{CO}_2 + \text{H}$
 147) $\text{OH} + \text{HCO} \rightarrow \text{H}_2\text{O} + \text{CO}$
 148) $\text{OH} + \text{H}_2\text{CO} \rightarrow \text{HCO} + \text{H}_2\text{O}$
 149) $\text{OH} + \text{CH}_3\text{O} \rightarrow \text{H}_2\text{O} + \text{H}_2\text{CO}$
 150) $\text{OH} + \text{CH}_3\text{OOH} \rightarrow \text{CH}_3\text{O}_2 + \text{H}_2\text{O}$
 151) $\text{HO}_2 + \text{O}_3 \rightarrow \text{OH} + 2\text{O}_2$
 152) $2\text{HO}_2 \rightarrow \text{H}_2\text{O}_2 + \text{O}_2$
 153) $2\text{HO}_2 \rightarrow \text{H}_2\text{O}_2 + \text{O}_2(^1\Delta)$
 154) $2\text{HO}_2 + \text{M} \rightarrow \text{H}_2\text{O}_2 + \text{O}_2 + \text{M}$
 155) $\text{HO}_2 + \text{NO} \rightarrow \text{NO}_2 + \text{OH}$
 156) $\text{HO}_2 + \text{NO}_2 + \text{M} \rightarrow \text{HO}_2\text{NO}_2 + \text{M}$
 157) $\text{HO}_2 + \text{NO}_3 \rightarrow \text{HNO}_3 + \text{O}_2$
 158) $\text{HO}_2 + \text{HCO} \rightarrow \text{H}_2\text{CO} + \text{O}_2$
 159) $\text{HO}_2 + \text{CH}_3\text{O} \rightarrow \text{H}_2\text{CO} + \text{H}_2\text{O}_2$
 160) $\text{HO}_2 + \text{CH}_3\text{O}_2 \rightarrow \text{CH}_3\text{OOH} + \text{O}_2$
 161) $\text{N} + \text{O}_2 \rightarrow \text{NO} + \text{O}$
 162) $\text{N} + \text{O}_3 \rightarrow \text{NO} + \text{O}_2$
 163) $\text{N} + \text{OH} \rightarrow \text{NO} + \text{H}$
 164) $\text{N} + \text{HO}_2 \rightarrow \text{NO} + \text{OH}$
 165) $2\text{N} + \text{M} \rightarrow \text{N}_2 + \text{M}$
 166) $\text{N} + \text{NO} \rightarrow \text{N}_2 + \text{O}$
 167) $\text{N} + \text{NO}_2 \rightarrow \text{N}_2\text{O} + \text{O}$
 168) $\text{N}_2 \rightarrow 2\text{N}$
 169) $\text{NO} + \text{NO}_3 \rightarrow 2\text{NO}_2$
 170) $\text{NO} + \text{CH}_3\text{O}_2 \rightarrow \text{CH}_3\text{O} + \text{NO}_2$
 171) $\text{NO}_3 + \text{NO}_2 \rightarrow \text{NO} + \text{NO}_2 + \text{O}_2$
 172) $\text{NO}_3 + \text{NO}_2 + \text{M} \rightarrow \text{N}_2\text{O}_5 + \text{M}$
 173) $2\text{NO}_3 \rightarrow 2\text{NO}_2 + \text{O}_2$
 174) $\text{N}_2\text{O}_5 + \text{H}_2\text{O} \rightarrow 2\text{HNO}_3$
 175) $\text{N}_2\text{O}_5 + \text{M} \rightarrow \text{NO}_3 + \text{NO}_2 + \text{M}$
 176) $\text{HO}_2\text{NO}_2 + \text{M} \rightarrow \text{HO}_2 + \text{NO}_2 + \text{M}$
 177) $\text{CH}_3 + \text{O}_2 \rightarrow \text{H}_2\text{CO} + \text{OH}$
 178) $\text{H}_3 + \text{O}_2 + \text{M} \rightarrow \text{CH}_3\text{O}_2 + \text{M}$
 179) $\text{CH}_3 + \text{O}_3 \rightarrow \text{CH}_3\text{O} + \text{O}_2$
 180) $\text{CH}_3 + \text{H}_2 \rightarrow \text{CH}_4 + \text{H}$
 181) $\text{CH}_3 + \text{HO}_2 \rightarrow \text{CH}_4 + \text{O}_2$
 182) $\text{CH}_3 + \text{HO}_2 \rightarrow \text{CH}_3\text{O} + \text{OH}$
 183) $\text{CH}_3 + \text{H}_2\text{O}_2 \rightarrow \text{CH}_4 + \text{HO}_2$
 184) $\text{CH}_3 + \text{HCO} \rightarrow \text{CH}_4 + \text{CO}$
 185) $\text{CH}_3 + \text{H}_2\text{CO} \rightarrow \text{CH}_4 + \text{HCO}$
 186) $\text{CH}_3 + \text{CH}_3\text{O} \rightarrow \text{H}_2\text{CO} + \text{CH}_4$
 187) $\text{CO} + \text{NO}_3 \rightarrow \text{NO}_2 + \text{CO}_2$
 188) $\text{HCO} + \text{O}_2 \rightarrow \text{CO} + \text{HO}_2$
 189) $2\text{HCO} \rightarrow \text{H}_2\text{CO} + \text{CO}$
 190) $\text{HCO} + \text{H}_2\text{CO} \rightarrow \text{CH}_3\text{O} + \text{CO}$
 191) $\text{H}_2\text{CO} + \text{NO}_3 \rightarrow \text{HCO} + \text{HNO}_3$
 192) $\text{CH}_3\text{O} + \text{O}_2 \rightarrow \text{H}_2\text{CO} + \text{HO}_2$
 193) $\text{CH}_3\text{O} + \text{CO} \rightarrow \text{CH}_3 + \text{CO}_2$
 194) $\text{CH}_3\text{O}_2 + \text{O}_3 \rightarrow 2\text{O}_2 + \text{CH}_3\text{O}$
 195) $2\text{CH}_3\text{O}_2 \rightarrow 2\text{CH}_3\text{O} + \text{O}_2$